Preprints of the 19th World Congress
The International Federation of Automatic Control
Cape Town, South Africa. August 24-29, 2014

Minimum-time Path Following in Highly Redundant Electric Vehicles

Ricardo de Castro [*] **Mara Tanelli** [**] **Rui Esteves Araújo** [***] **Sergio M. Savaresi** [**]

[*] *R. de Castro is with the Institute of System Dynamics and Control, German Aerospace Center (DLR), 82234 Wessling, Germany*
[**] *M. Tanelli and S. M. Savaresi are with the Dipartimento di Elettronica, Informazione e Bioingegneria, Politecnico di Milano, Piazza Leonardo da Vinci 32, 20133 Milano, Italy. Corresponding author: Mara Tanelli, mara.tanelli@polimi.it*
[***] *R. Esteves Araújo is with Faculdade de Engenharia da Universidade do Porto, Rua Dr. Roberto Frias, s/n 4200-465 Porto, Portugal*

Abstract: Autonomous vehicles are becoming a reality that in the next future will most probably start populating everyday roads. Such vehicles can, on the one hand, increase safety through automated driving, and, on the other, be a means of transportation also for people with disabilities who cannot move alone on commercial cars. Within this class of vehicles, mechanical layouts that allow an actuator redundancy coupled with electric propulsion appear particularly interesting, as they make it possible to design motion controller that can optimally blend multiple objectives, both dynamic, safety and driver-oriented. This paper considers such setting and concentrates on the design of a path-following algorithm with minimum-time features, with the aim of combining performance and energy-oriented optimization of the vehicle motion. The effectiveness of the approach is assessed by means of simulation tests carried out on the CarSim vehicle simulation environment.

1. INTRODUCTION

Active vehicle dynamics controllers, introduced in commercial cars during the 1980s with anti-lock braking systems, [Savaresi and Tanelli, 2010] and traction controllers, and extended more recently with lateral stability control systems, [van Zanten, 2002], are recognized today as indispensable tools to ensure safe motion of the vehicle. The next generation of electronic aids is expected to evolve toward the full automation of the vehicle and, eventually, the release of humans from driving duties. This can bring enormous benefits to vehicle users. To start with, releasing the driver from the tedious manual driving operations may allow focusing on more productive and enjoyable tasks, [Coelingh and Solyom, 2012]. From a safety point of view, cars that are "impossible" to crash can be envisioned, which can further reduce road fatalities. From a social standpoint, the possibility of having disabled people (*e.g.*, visually impaired) driving without the assistance of other humans represents another example of the impact that such technologies can bring to people's lives [Urmson, 2012].

Within this interesting context, the present work focuses on path-following controller, with particular attention to vehicle configurations with highly redundant actuators. The main challenge in the development of path-following algorithms for ground vehicle lies in the complexity of the dynamic models, especially for the nonlinear mechanisms associated with the friction forces between the tyre and road. One way to deal with such issues is to rely on idealized assumptions, derived mainly from the mobile robots literature, such as pure rolling of the tyres and zero side-slip, to derive simple, but practical, vehicle kinematic models, [Morin and Samson, 2008], which can be possibly extended to comprise the actuators dynamics, as discussed in *e.g.*, [Werling et al., 2010]. Nonetheless, since these approaches do not take into account the tyre-road friction forces, together with the limited validity of pure-rolling and zero side-slips assumptions, they end up confining the applicability of kinematic-based controllers to low-speed manoeuvres, [Werling et al., 2010]. To improve such models, approaches have been proposed which make use of the bicycle model, see *e.g.*, [Ferrara and Vecchio, 2009]. The main shortcoming in this case is related to the assumption that the lateral and longitudinal vehicle dynamics are decoupled, which forces to design the path following algorithm under the assumption that the vehicle longitudinal speed is constant through the corners, imposed by a (longitudinal) velocity regulator that operates independently from the lateral motion controller.

To overcome these limitations, the proposed path following controller will employ a nonlinear two-track vehicle model, with nonlinear tyre forces and dynamic load transfer. Although this leads to increased modeling complexity, it will be shown that the model can be effectively employed and that it is instrumental to allow the path-following controller to operate the vehicle near its adhesion limits. The redundant architecture, with four in-wheel-motors (4IWM) and four wheel-steer (4WS) is the enabling technology that allows us to handle, within a nonlinear framework, the min-time path following problem.

The main contributions of the work are the adaptation to automotive applications of the convex formulation of the minimum-time path following problems that was devised in robotics [Verscheure et al., 2009][Pfeiffer and Johanni, 1987]. It will be shown that, thanks to the specific vehicle platform, we can explore trade-offs between performance and energy consumption. Specifically, for a given, pre-specified path, the user can configure the controller so that the vehicle travels through the path *i*) in minimum-time; *ii*) with minimum-energy; or *iii*) pursuing trade-off between the two. Consequently, in contrast to the classical path-following setting in which the vehicle velocity is kept

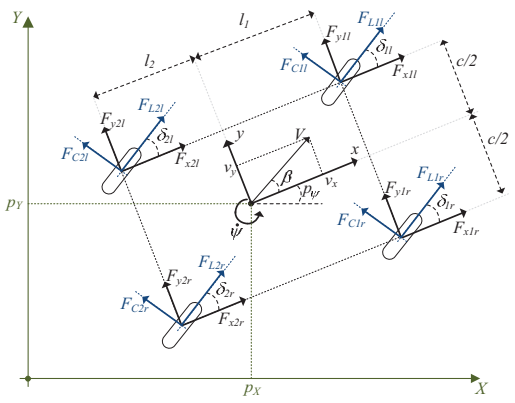

Fig. 1. Two-track vehicle model.

constant, [Morin and Samson, 2008], the proposed controller generates appropriate speed profiles that take into account the adhesion limits of the car and the user's preferences (lap-time *vs* energy consumption).

2. VEHICLE DYNAMICS MODEL

A two-track nonlinear vehicle model will be presented, composed of 4 independent wheel drive, and 4 independent wheel steering. To make the model tractable, the roll and pitch dynamics of the EV will be neglected. The dynamic evolution of the vehicle position $\mathbf{p}$

$$\mathbf{p} = \begin{bmatrix} \mathrm{p}_X & \mathrm{p}_Y & \mathrm{p}_\psi \end{bmatrix}^T, \tag{1}$$

where the XY axis is fixed with the Earth and p_ψ is the angle between the vehicle orientation and the X axis, *i.e.*, the yaw-angle, is defined as

$$\mathbf{M}\ddot{\mathbf{p}} = \mathbf{T}(\mathbf{p})\left(\mathscr{F} - \mathscr{R}(\mathbf{p},\dot{\mathbf{p}}) + \mathscr{D}\right), \tag{2}$$

where $\mathbf{M} = \mathrm{diag}([m,m,I_z])$, m is the vehicle mass, I_z the yaw inertia, $\mathscr{D} \in \mathbb{R}^3$ a generalized force due to the effect non-modeled dynamics and disturbances, $\mathscr{R}(\cdot) \in \mathbb{R}^3$ are resistance forces opposing the vehicle motion, and $\mathscr{F}$ are the centre of gravity (CoG) forces

$$\mathscr{F} = \begin{bmatrix} F_x & F_y & M_z \end{bmatrix}^T \in \mathfrak{F} \subset \mathbb{R}^3, \tag{3}$$

with F_x being the longitudinal force, F_y the lateral force and M_z the yaw-moment. In the sequel, it will be assumed that the resistance forces can be decomposed into two components

$$\mathscr{R}(\mathbf{p},\dot{\mathbf{p}}) = \mathscr{R}_1 + \mathscr{R}_2(\mathbf{p},\dot{\mathbf{p}})\dot{\mathbf{p}}, \tag{4}$$

where $\mathscr{R}_1 \in \mathbb{R}^3$ is a constant term due to rolling resistance and $\mathscr{R}_2(\mathbf{p},\dot{\mathbf{p}}) \in \mathbb{R}^3$ is a resistance term related with the aerodynamic drag. With respect to this last component, it will be further considered that, for $\alpha \geq 0$,

$$\mathscr{R}_2(\mathbf{p},\alpha\dot{\mathbf{p}}) = \alpha\mathscr{R}_2(\mathbf{p},\dot{\mathbf{p}}). \tag{5}$$

The matrix $\mathbf{T}(\mathbf{p})$ employed in (2), represents a transformation between variables expressed in the vehicle local frame and the XY axis. For example, the vehicle velocity expressed in the local coordinates $\mathbf{v} = \begin{bmatrix} v_x & v_y & \dot{\psi} \end{bmatrix}^T$ (*i.e.*, longitudinal, lateral and yaw velocity) is related to $d\mathbf{p}/dt$ through

$$\frac{d\,\mathbf{p}}{dt} = \begin{bmatrix} \cos(\mathrm{p}_\psi) & -\sin(\mathrm{p}_\psi) & 0 \\ \sin(\mathrm{p}_\psi) & \cos(\mathrm{p}_\psi) & 0 \\ 0 & 0 & 1 \end{bmatrix} \mathbf{v} = \mathbf{T}(\mathbf{p})\mathbf{v} \tag{6}$$

The generalized force/moments $\mathscr{F}$ are a direct consequence of the individual friction forces, F_{Li}, F_{Ci}, generated by each tyre (see Fig. 1), while the set $\mathfrak{F}$ in (3) represents the admissible set of force/moments that can be applied to the CoG. To model these forces, a simplified version of the well-known magic tyre formula [Pacejka, 2002] will be employed, yielding the combined-slip description used in [de Castro et al., 2013].

Remark 2.1. The longitudinal (F_{Li}) and cornering (F_{Ci}) forces of the tyre must fulfil

$$F_{Li}^2 + F_{Ci}^2 = F_i^2 \leq (\mu_{max}F_{zi})^2, \quad i \in \mathfrak{T}, \tag{7}$$

where $\mathfrak{T} = \{1l, 1r, 2l, 2r\}$ is set of indexes associated with the vehicle wheels. The previous result is known in the literature as the friction circle constraint [1], and essentially states that the force generated by the tyre must lie within a circle with a radius defined by the vertical load and the friction peak μ_{max}. The friction circle constraint also holds for the forces defined in the xy coordinates

Remark 2.2. the forces F_{xi}, F_{yi} are confined to the following set

$$F_{xi}^2 + F_{yi}^2 = \left\| \mathbf{W}(\delta_i) \begin{bmatrix} F_{Li} \\ F_{Ci} \end{bmatrix} \right\|_2^2 = F_i^2 \leq (\mu_{max}F_{zi})^2, \quad i \in \mathfrak{T},$$

where $\mathbf{W}(\delta_i)$ is a rotation matrix that realizes the change of coordinates and does not affect the tyre force magnitude.

The tyre vertical forces F_{zi} are affected by the load transfer between front and rear axles and left-right wheels that the vehicle experiences when subject to longitudinal and lateral accelerations. To model these factors, the following quasi-static mapping will be used, [Kiencke and Nielsen, 2005]

$$\mathbf{F}_z = \mathbf{F}_z^0 + \rho_x a_x + \rho_y a_y, \tag{8}$$

$$\mathbf{F}_z = \begin{bmatrix} F_{z1l} & F_{z1r} & F_{z2l} & F_{z2r} \end{bmatrix}^T, \quad \mathbf{F}_z^0 = \frac{mg}{2(l_1+l_2)} \begin{bmatrix} l_2 & l_2 & l_1 & l_1 \end{bmatrix}^T$$

$$\rho_x = \frac{mh}{2(l_1+l_2)} \begin{bmatrix} -1 & -1 & 1 & 1 \end{bmatrix}^T$$

$$\rho_y = \frac{mh}{c(l_1+l_2)} \begin{bmatrix} -l_2k_f & l_2k_f & -l_1k_r & l_1k_r \end{bmatrix}^T,$$

where $\mathbf{F}_z^0$ is the static force distribution, h the height of the CoG, k_f, k_r represent the front and rear coefficients associated with the lateral load transfer due to vehicle roll (see [Gillespie, 1992]), g is the gravitational acceleration, (l_1, l_2) characterize the position of the CoG (see Fig. 1) and a_x, a_y the vehicle longitudinal and lateral accelerations, respectively

$$\begin{bmatrix} a_x \\ a_y \end{bmatrix} = \begin{bmatrix} \frac{1}{m} & 0 & 0 \\ 0 & \frac{1}{m} & 0 \end{bmatrix} \left(\mathscr{F} - \mathscr{R}(\mathbf{p},\dot{\mathbf{p}})\right). \tag{9}$$

The rotational dynamics of each wheel is given by

$$J\dot{\omega}_i = T_i - r_iF_{Li}, \qquad i \in \mathfrak{T},$$

where J is the wheel inertia, and T_i the wheel torque, generated by a combination of IWM ($T_{m,i}$) and brake-by-wire actuators ($T_{b,i}$), *i.e.*, $T_i = T_{m,i} + T_{b,i}$. The main limiting factors in the actuators are the acceleration power and acceleration torque limits associated with the IWM, yielding

$$\underline{T} \leq T_i \leq \overline{T}, \quad T_i\omega_i \leq \overline{P}, \qquad i \in \mathfrak{T}, \tag{10}$$

where $\overline{T} \in \mathbb{R}_+$ is the maximum acceleration torque that the motor can develop, $\underline{T} \in \mathbb{R}_-$ the maximum braking torque of the brake-by-wire system, and $\overline{P}$ the maximum acceleration power,

[1] For simplicity, the representation of the tyre-road friction forces considered here assumes an isotropic condition, which leads to the friction circle constraint instead of an elliptic one.

which are assumed to be equal for all wheels. The braking power limits are not explicitly considered here, since, due to safety concerns, modern braking systems are generally able to reach the friction limits. Further, it is assumed that each wheel has independent steering capabilities, constrained to the following sets

$$-\overline{\delta} \leq \delta_i \leq \overline{\delta}, \qquad i \in \mathfrak{T}, \tag{11}$$

where $\overline{\delta}$ is the maximum steering range.

In summary, the vehicle model can be compactly represented as

$$\mathbf{M}\ddot{\mathbf{p}} = \mathbf{T}(\mathbf{p})\left(\mathscr{F} - \mathscr{R}(\mathbf{p},\dot{\mathbf{p}}) + \mathscr{D}\right) \tag{12a}$$

$$\mathscr{F} = \mathbf{B}\,\mathbf{F}_{\mathrm{xy}} \tag{12b}$$

$$\mathbf{F}_{\mathrm{xy_i}} = \mathbf{W}(\delta_i)\left[F_{Li}\ \ F_{Ci}\right]^T, \quad i \in \mathfrak{T} \tag{12c}$$

$$\begin{bmatrix} F_{Li} \\ F_{Ci} \end{bmatrix} = \tilde{\mathbf{F}}_i(\mathbf{p},\dot{\mathbf{p}},\omega_i,\delta_i,F_{zi},\theta_T), \qquad i \in \mathfrak{T} \tag{12d}$$

$$\mathbf{F}_z = \mathbf{F}_z^0 + \frac{\rho_x}{m}\mathbf{e}_1^T(\mathscr{F} - \mathscr{R}) + \frac{\rho_y}{m}\mathbf{e}_2^T(\mathscr{F} - \mathscr{R}) \tag{12e}$$

$$J\dot{\omega}_i = T_i - r_i F_{Li}, \qquad i \in \mathfrak{T} \tag{12f}$$

$$\underline{T} \leq T_i \leq \overline{T}, \quad T_i\omega_i \leq \overline{P}, \quad -\overline{\delta} \leq \delta_i \leq \overline{\delta}, \quad i \in \mathfrak{T} \tag{12g}$$

where $\tilde{\mathbf{F}}_i \in \mathbb{R}^2$ is the friction force, θ_T represents the parameters of the friction model, $\mathbf{F}_{\mathrm{xy_i}}$ refers to the x and y force components of the tyre $i \in \mathfrak{T}$, and $\mathbf{e}_1^T = [1\ 0\ 0]^T$, $\mathbf{e}_2^T = [0\ 1\ 0]^T$. In the previous equations, the $\mathbf{B}$ matrix transforms the wheel forces $\mathbf{F}_{\mathrm{xy}}$ to CoG forces, while $\mathbf{W}(\delta_i)$ is a change of coordinates between tyre and vehicle frame (see de Castro et al. [2013] for the formal definition of these variables).

3. PATH-FOLLOWING CONTROLLER

As shown in Fig. 2, the path-following controller proposed in this work is composed of three components *i*) an optimal feedforward (FF) term; *ii*) a cascade position-speed control loop; and *iii*) a force allocation block. The main input of this controller is the reference path $\mathbf{p}_r(s)$ - assumed to be smooth - that the vehicle should follow. To qualitatively specify how fast the vehicle should go through the reference path, the user (or the path planning layer) provides the parameter $\varepsilon \in [0,1]$, which represents a trade-off factor between the journey time and the energy consumption of the vehicle. This information is then used by the optimal FF to generate a suitable speed profile $\mathbf{v}_r(t)$, considering both the vehicle dynamics constraints and the adhesion level at the tyre-road interface $\hat{\mu}_{max}$, which may be provided from a dedicated friction peak observer. Additionally, the optimal FF also produces an estimate of the CoG forces and moments $\mathscr{F}_r$, which, in absence of modeling errors, would be enough to achieve a perfect tracking of $\mathbf{v}_r(t)$. However, to cope with modeling uncertainties and external disturbances, the position and speed loops operate in parallel to the optimal FF in a cascade setting. More specifically, the position loop generates speed increments to be superimposed to the speed profile $\mathbf{v}_r(t)$, while the speed loop manipulates force increments that are added to $\mathscr{F}_r(t)$.

3.1 Optimal Feedforward

Construction of the Attainable Set of Forces The first issue that needs to be addressed is the construction of the admissible set of forces and moments, *i.e.*, $\mathfrak{F} \subset \mathbb{R}^3$, achievable by the vehicle. In our formulation, this attainable set is dominated by the friction constraints ($\mathfrak{F}_f$), as well as the torque and power limits imposed by the IWMs ($\mathfrak{F}_T$)

$$\mathfrak{F} = \mathfrak{F}_f \bigcap \mathfrak{F}_T. \tag{13}$$

As far as the friction constraints are concerned, it is worth recalling Remark 2.2, which states that the tyre friction limits in the xy components are dependent on the friction peak μ_{max} and on the vertical load (F_{zi}). Thus $\mathfrak{F}_f$ might be defined as

$$\begin{aligned} \mathfrak{F}_f = \{\, \mathscr{F} = \mathbf{B}\,\mathbf{F}_{\mathrm{xy}} \in \mathbb{R}^3 \quad | \quad \forall i \in \mathfrak{T} \\ \|\mathbf{E}_i\,\mathbf{F}_{\mathrm{xy}}\|_2 \leq \mu_{max} F_{zi} \\ = \mu_{max}\left(F_{zi}^0 + \left(\frac{\rho_{xi}}{m}\mathbf{e}_1^T + \frac{\rho_{yi}}{m}\mathbf{e}_2^T\right)\mathbf{B}\,\mathbf{F}_{\mathrm{xy}}\right),\} \end{aligned} \tag{14}$$

where $\mathbf{E}_i \in \mathbb{R}^{2\times 8}$ is a matrix that extracts the x and y components associated with the tyre $i \in \mathfrak{T}$. To keep the analysis simple, the influence of the resistance forces $\mathscr{R}$ were neglected in the calculation of the vertical forces F_{zi}.

Remark 3.1. $\mathfrak{F}_f$ is a convex set in $\mathbb{R}^3$.

As for the power and torque constraints introduced by IWMs, we will approximate them using the following set

$$\mathfrak{F}_T(v_x) \approx \{\mathscr{F} = [F_x\ F_y\ M_z]^T, \mid F_x \leq n_T\overline{F}, \quad F_x v_x \leq n_T\overline{P}\} \tag{15}$$

where $n_T = 4$, $\overline{F} = \overline{T}/r_i$. The basic idea of the above formulation is to translate the torque and power limits of the wheel-motors to the CoG longitudinal force and speed.

Path Following Problem As a starting point for the design of the optimal FF controller, it is worth noticing that, if the equations of motion were ideal ($\mathscr{D} \equiv 0$), and if the position error at the initial instant zero ($\mathbf{p}(0) = \mathbf{p}_r(0)$, then the perfect tracking of $\mathbf{p}_r$ would be ensured if

$$\left(\mathbf{T}^{-1}(\mathbf{p}_r)\,\mathbf{M}\right)\ddot{\mathbf{p}}_r + \mathscr{R}_2(\mathbf{p}_r,\dot{\mathbf{p}}_r)\dot{\mathbf{p}}_r + \mathscr{R}_1 = \mathscr{F}_r, \quad \mathscr{F}_r \in \mathfrak{F} \tag{16}$$

where $\mathscr{F}_r$ is the feedforward force term. Given that the reference path is specified in the path coordinate s, i.e. $\mathbf{p}_r(s)$, the first and second time derivative of $\mathbf{p}_r$ take the form

$$\dot{\mathbf{p}}_r(s) = \frac{d\,\mathbf{p}_r(s)}{dt} = \frac{d\,\mathbf{p}_r(s)}{ds}\frac{ds}{dt} = \mathbf{p}_r'(s)\dot{s} \tag{17}$$

$$\ddot{\mathbf{p}}_r(s) = \frac{d^2\,\mathbf{p}_r(s)}{dt^2} = \mathbf{p}_r''(s)\dot{s}^2 + \mathbf{p}_r'(s)\ddot{s}. \tag{18}$$

Inserting these relations into (16), and after some straightforward algebraic manipulations, one gets

$$\mathbf{m}(s)\ddot{s} + \mathbf{r}_2(s)\dot{s}^2 + \mathbf{r}_1 = \mathscr{F}_r, \quad \mathscr{F}_r \in \mathfrak{F}, \tag{19}$$

where

$$\begin{aligned} \mathbf{m}(s) &= \mathbf{T}^{-1}(\mathbf{p}_r(s))\,\mathbf{M}\,\mathbf{p}_r'(s) \\ \mathbf{r}_2(s) &= \mathbf{T}^{-1}(\mathbf{p}_r(s))\,\mathbf{M}\,\mathbf{p}_r''(s) + \mathscr{R}_2(\mathbf{p}_r(s),\mathbf{p}_r'(s))\,\mathbf{p}_r'(s) \\ \mathbf{r}_1 &= \mathscr{R}_1\,. \end{aligned} \tag{20}$$

Notice that, to determine $\mathbf{r}_2$, (5) and the fact that $\dot{s} > 0$ (speed reversals along the reference path are not allowed) were used. Finally, the vehicle speed (in the local coordinates) can also be expressed as a function of s in the form

$$\mathbf{v}_r(s) = \mathbf{T}^{-1}(\mathbf{p}_r(s))\,\mathbf{p}_r'(s)\dot{s} = \tilde{\mathbf{v}}_r(s)\dot{s}. \tag{21}$$

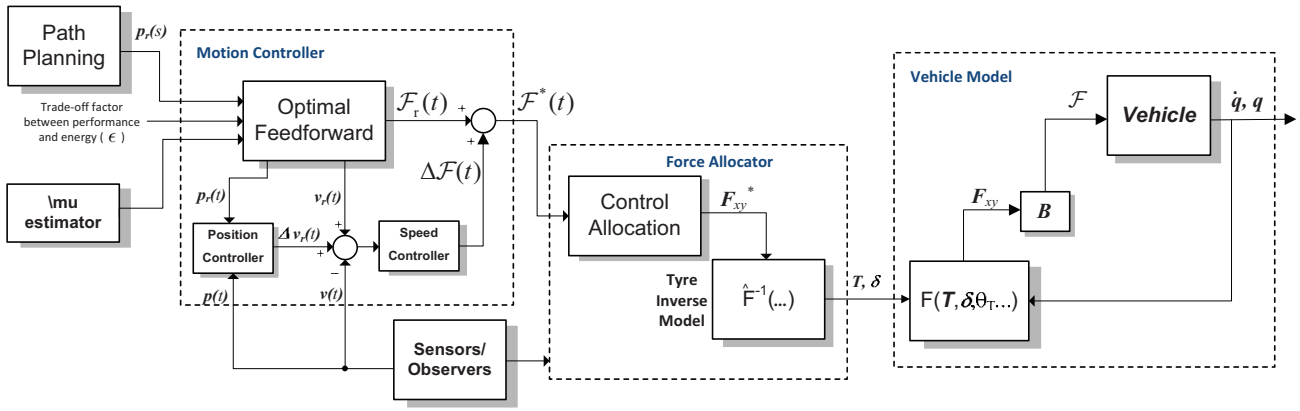

Fig. 2. Block diagram of the proposed control algorithm.

Convexification We will now discuss a series of practical modifications, which will ultimately lead to a convex formulation of the optimal feedforward controller. First, the change of independent variable suggested in [Pfeiffer and Johanni, 1987, Verscheure et al., 2009] will be adopted: instead of time (t), we will consider the normalized distance in the reference path, s, as independent variable. This means that $\dot{s} = ds/dt$, which enables us to rewrite the journey time as

$$T = \int_0^T 1dt = \int_{s(0)}^{s(T)} \frac{ds}{\dot{s}} = \int_0^1 \frac{1}{\dot{s}} ds. \tag{22}$$

Furthermore, with this change of variable, the terms $\ddot{s}$ and $\dot{s}^2$ appear linearly in (19). This observation leads to a second change of variable, [Pfeiffer and Johanni, 1987, Verscheure et al., 2009]

$$a(s) = \ddot{s}^2, \quad b(s) = \dot{s}^2, \tag{23}$$

where

$$a(s) = \frac{d\dot{s}}{dt} = \dot{s}\frac{d\dot{s}}{ds} = \frac{1}{2}\frac{d\dot{s}^2}{ds} = \frac{1}{2}\frac{d(b(s))}{ds}. \tag{24}$$

Thus, with the introduction of $a(s)$ and $b(s)$, the nonlinear differential relation (19) is decoupled into two parts: one affine constraint ($\mathbf{m}(s)a + \mathbf{r}_2(s)b + \mathbf{r}_1 = \mathscr{F}_r$), and one linear differential equation (24).

Another aspect that deserves discussion is the convexity of the admissible set $\mathfrak{F}$, which is the result of the friction limits ($\mathfrak{F}_f$) and the torque/power constraints of the electric motors ($\mathfrak{F}_T(v_x)$). While the convexity of $\mathfrak{F}_f$ was already established in Remark 3.1, the set $\mathfrak{F}_T(v_x)$ requires further analysis. From (15), it is clear that the power and torque limits affect mainly the F_x component of $\mathscr{F}$; thus, it is more practical to analyse these constraints in the domain (v_x,F_x), *i.e.*,

$$\Omega_T = \{(v_x, F_x) \in \mathbb{R}^2 \,:\, F_x v_x \le n_T \overline{P}, \quad F_x \le n_T \overline{F}\}. \tag{25}$$

As depicted in Fig. 3.1.3, when the vehicle exceeds the nominal speed $V_n = \overline{P}/\overline{F}$ the power constraints make the set Ω_T non-convex, which is a relevant obstacle to the determination of a global optimal solution for the optimization problem, [Boyd and Vandenberghe, 2004]. To mitigate this issue, a convexification technique will be used to handle the power constraint. The idea is to approximate the non-convex constraint $F_x v_x \le n_T \overline{P}$ with a linear inequality, characterized by the points $(\underline{V}, n_T\overline{F})$, and $(\overline{V}, n_T\overline{P}/\overline{V})$. The points $\underline{V} \le V_n$ and $\overline{V} \ge V_n$ are tuning parameters: a wise rule of thumb is to select $\overline{V}$ close to the point where the aerodynamic drag overcomes the maximum

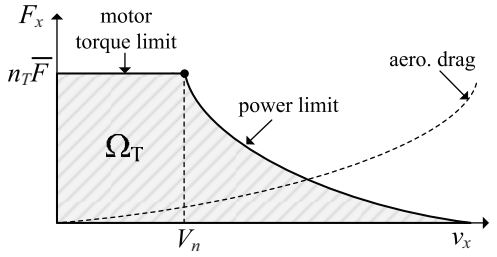

Fig. 3. Non-convex set of the power limits introduced by the electric motors.

power of the vehicle. The linear approximation of Ω_T can also be expressed as

$$\hat{\Omega}_T = \{(v_x, F_x) \,:\, F_x \le (v_x - \underline{V})\tilde{\gamma}_p + n_T\overline{F}, \quad F_x \le n_T\overline{F}\}$$

where $\tilde{\gamma}_p = n_T \frac{\overline{P}/\overline{V} - \overline{F}}{\overline{V} - \underline{V}}$. Now, notice that, after introducing the new variable b, and taking into account (21), the vehicle longitudinal speed is given by $v_x = \mathbf{e_1}^T \tilde{\mathbf{v}}_r(s)\dot{s} = \mathbf{e_1}^T \tilde{\mathbf{v}}_r(s)\sqrt{b(s)}$. This implies that the power constraints in $\hat{\Omega}_T$, although being linear in v_x, become nonlinear when we include the new variable $b(s)$: in fact, they also lose the convexity property, which is even worse for our purposes here. This issue spurred us to find an alternative convexification technique that can be applied to the space $(F_x, b(s))$. With this goal in mind, it is convenient to first relate v_x and b as

$$b = \left(\frac{v_x}{\mathbf{e_1}^T \tilde{\mathbf{v}}_r(s)}\right)^2. \tag{26}$$

Now, recall that the linear approximation in (F_x, v_x) was characterized by a half-plane that passes through the points $(\underline{V}, n_T\overline{F})$, $(\overline{V}, n_T\overline{P}/\overline{V})$. One alternative way of dealing with the linear approximation with $b(s)$ is to translate this half-plane to the space $((F_x, b(s))$, using, for that purpose, the relation (26). The resulting linear approximation of the power constraint is then obtained as

$$F_x \le \gamma_p(s)(b - \underline{b}(s)) + n_T\overline{F}, \quad \gamma_p(s) = n_T \frac{\overline{P}/\overline{V} - \overline{F}}{\overline{b}(s) - \underline{b}(s)}. \tag{27}$$

where

$$\overline{b}(s) = \left(\frac{\overline{V}}{\mathbf{e_1}^T \tilde{\mathbf{v}}_r(s)}\right)^2, \quad \underline{b}(s) = \left(\frac{\underline{V}}{\mathbf{e_1}^T \tilde{\mathbf{v}}_r(s)}\right)^2. \tag{28}$$

Although this constraint will introduce approximation errors, it is a practical approach to handle the power limitation of the electric motors.

In the light of the above considerations, the final path following problem can be posed as

$$\begin{aligned}
&\min_{\mathscr{F}_r,a,b} \varepsilon \int_0^1 \frac{1}{\sqrt{b(s)}} ds + (1-\varepsilon) \int_0^1 \mathscr{F}_r(s)^T \mathbf{W} \mathscr{F}_r(s) ds \\
&s.t. \quad \mathbf{m}(s)a(s) + \mathbf{r}_2(s)b(s) + \mathbf{r}_1 = \mathscr{F}_r(s) \\
&\qquad \frac{d}{ds}b(s) = 2a(s), \quad b(0) = \dot{s}_0^2, \qquad b(s) > 0 \\
&\qquad \mathscr{F}_r(s) \in \mathfrak{F}_f, \qquad \mathbf{e}_1^T \mathscr{F}_r(s) \leq n_T \overline{F} \\
&\qquad \mathbf{e}_1^T \mathscr{F}_r(s) \leq \gamma_p(s)(b(s) - \underline{b}(s)) + n_T \overline{F}, \quad s \in [0, \overline{s}].
\end{aligned} \tag{29}$$

Notice that, to (indirectly) penalize the energy consumption, a quadratic term in the forces $\mathscr{F}_r$ was incorporated into the cost function. This penalization is controlled through the diagonal weight matrix $\mathbf{W} = \text{diag}\{w_1, w_2, w_3\}$ and the parameter $\varepsilon \in [0,1]$, which describes the trade-off factor between the min-time and the energy consumption goals.

Remark 3.2. The above optimization problem is convex.

This convex property was already pointed out by [Verscheure et al., 2009] in a robotic context, and it is extended here for the minimum-time path following of autonomous vehicles. In comparison with the minimum-time path-following problem of robotic manipulators, [Pfeiffer and Johanni, 1987, Verscheure et al., 2009], the main differences in the vehicle case are due to the power limits constraints ($\mathfrak{F}_T$) and friction circle ($\mathfrak{F}_f$).

Collocation Method To facilitate the resolution of (29), we adopted a direct optimization approach, also known as collocation [Betts, 2010]. This means that the dynamic equations in (29) were discretized (through the trapezoidal method), yielding a discrete optimization problem that was solved with the help of the SDPT3 numerical solver. After extracting the numerical solution, the time-domain variables can then be retrieved using the relation (22); variables of particular interest are the feedforward term $\mathscr{F}_r(t)$, the reference trajectory $\mathbf{p}_r(t)$ and the speed profile $\mathbf{v}_r(t)$.

3.2 Speed and Position Controller

In order to gain robustness against disturbances, the motion controller also incorporates a cascade position-speed feedback loop (see Fig. 2). The goal of this feedback loop is to track the speed profile $\mathbf{v}_r$ and position setpoint $\mathbf{p}_r$ - obtained during the optimization process -, using a corrective force demand $\Delta\mathscr{F}$ as virtual control input. Toward this goal, a sliding mode control law, endowed with conditional integrators, was employed in the design of the feedback loops. Due to space constraints, the details regarding the design of this controller are omitted here; the interest reader is referred to [de Castro, 2013] for additional information.

3.3 Force allocation

The last step in the controller design consists in allocating the CoG's force demands $\mathscr{F}^* = \mathscr{F}_r + \Delta\mathscr{F}$ into wheel torques T_i and steer angles δ_i. Given the high level of redundancy in the vehicle platform, the allocation solution is, in general, not unique, which paves the way to the pursuit of secondary goals, such as the minimization of the energy consumption of the actuators and/or the friction utilization of the tyres. In order tackle this challenge, our solution to the force allocation problem was decomposed into two steps. In the first step, we assumed that the *xy* forces of the tyres ($\mathbf{F}_{\text{xy}}$) can be independently controlled, *i.e.*, they can be regarded as a second virtual control. Based on this assumption, the *xy* force distribution was determined through a quadratic programming (QP) optimization problem, which targets the minimization of the tyre's friction usage, constrained by friction limits, power restrictions of the motors and (12b). The second step of the allocation process, relies on inversion of the tyre forces (not discussed here due to space limits), *i.e.*, using the $\mathbf{F}_{\text{xy}}$ obtained in the first allocation step, and the vehicle state $\mathbf{v}$, find the torque (T_i) and steer (δ_i) that produces the necessary tyre forces. Additional details on this force allocation process can be found in [de Castro, 2013].

4. SIMULATION RESULTS

To evaluate the performance of the proposed approach, simulation tests were carried out with the full vehicle model in the CarSim simulation environment. This allows us to test the robustness against unmodeled dynamics. The vehicle model is that of a B-Class sports car, available in the default CarSim library. It is assumed that the reference path is pre-specified before the start of the simulation, so that the convex optimal problem in the motion controller is solved (off-line) generating the FF components $\mathscr{F}_r$, $\mathbf{v}_r$, $\mathbf{p}_r$. Further, Gaussian noises were added to the measured variables. The speed and position feedback loops, together with the control-allocation layer, impose (on-line) the tracking of this pre-specified motion. The default settings employed in the simulation are: i) zero vehicle side-slip reference; ii) $\mu_{max} = 1$: dry asphalt; iii) $\varepsilon = 1$: minimum-time goal; iv) equal penalization for all the forces.

To test the performance on a varied track, the 2.2km Norising circuit was used. The results of the minimum-time path following for this track are presented in Fig. 4. By inspecting the subfigures, one may note that *i*) the tracking errors are small, with a peak position error smaller than 0.5m, *ii*) the FF components generated by the optimal approach produce a control action that is very close to the feedback term (particularly as far as v_x and v_y are concerned), which proves the usefulness of the FF in achieving good control performance; and *iii*) the torque distribution between the four wheels is largely dependent on the load transfer that the vehicle is subject to, *i.e.*, the wheels with larger vertical load receive more torque so as to keep the overall friction use low. Taking into account the control allocation formulation, which aims to minimize the friction use, the allocation results agree with the expectations. Further, to evaluate the trade-off between energy and performance metrics along the track, Fig. 5 shows the energy vs. performance trade-off curve, which demonstrates that, if the user is willing to sacrifice lap-time, the energy gains can be very significant, *e.g.*, increasing the lap-time by 20% allows energy savings up to 55%.

5. CONCLUDING REMARKS AND OUTLOOK

In this work, a path following algorithm for highly redundant electric vehicles, endowed with 4IWMs and 4WS, was proposed. It is composed of a multi-layer control architecture that takes care of the vehicle motion control and of the force allocation step, allowing a multi-objective optimization which is enabled by the actuator redundancy. Simulation results carried out in the high-fidelity CarSim simulator demonstrated the effectiveness of the overall approach, both in normal driving condition, and in extreme conditions (with high side-slip). Sensitive studies also revealed the trade-offs between lap-time and

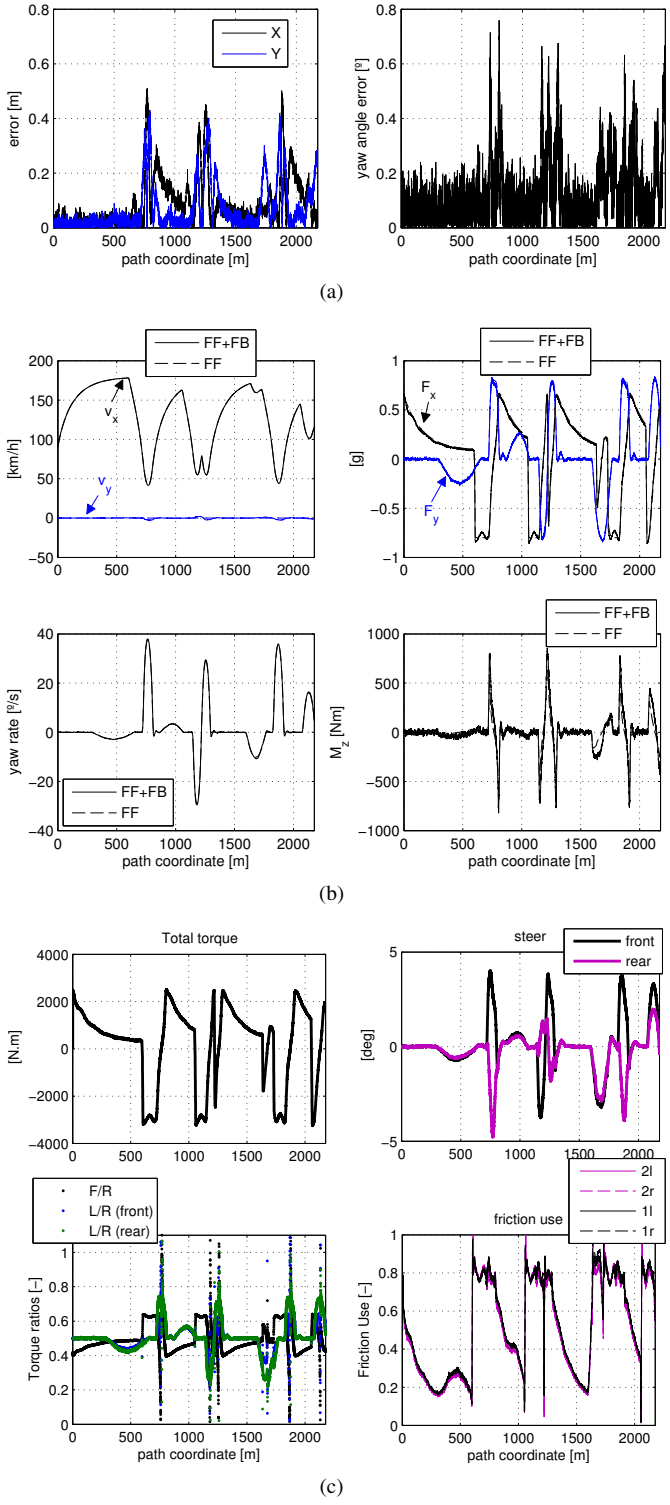

Fig. 4. Simulation results for the track evaluation.

energy consumption that the path following controller can provide. Future work will address the interaction between the path following algorithm with the path-planning layer, using real-time solvers for the generation of the feed-forward component of the motion controller.

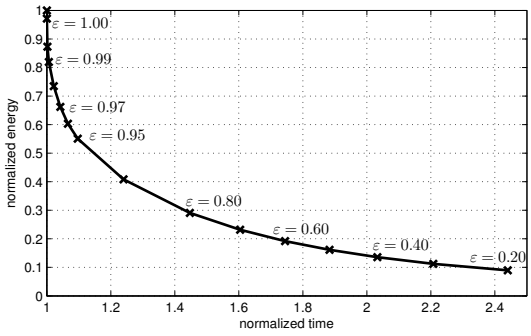

Fig. 5. Influence of the parameter ε in the energy consumption and lap-time performance in the track simulations.

REFERENCES

J.T. Betts. *Practical methods for optimal control and estimation using nonlinear programming*. Society for Industrial and Applied Mathematics, 2010.

Stephen Boyd and Lieven Vandenberghe. *Convex Optimization*. Cambridge University Press, 2004.

Erik Coelingh and Stefan Solyom. All aboard the robotic road train. *IEEE Spectrum*, 49(11):34–39, 2012.

R. de Castro. *Motion Control and Energy Management of Electric Vehicles*. PhD thesis, Faculdade de Engenharia da Universidade do Porto, 2013.

R. de Castro, M. Tanelli, R.E. Araujo, S. Savaresi, and D. Freitas. Torque allocation in evs with 4 in-wheel motors: a high-performance approach. In *Proceedings of the 23nd International Symposium on Dynamics of Vehicles on Roads and Tracks (IAVSD13)*, Qingdao, China, 2013.

A. Ferrara and C. Vecchio. Second order sliding mode control of vehicles with distributed collision avoidance capabilities. *Mechatronics*, 19(4):471–477, 2009.

Thomas D. Gillespie. *Fundamentals of Vehicle Dynamics*. Society of Automotive Engineers, Inc., 1992.

U. Kiencke and L. Nielsen. *Automotive Control Systems For Engine, Driveline, and Vehicle*. Springer-Verlag, 2005.

P. Morin and C. Samson. Motion control of wheeled mobile robots. In *Handbook of Robotics*, pages 799–826. Springer Berlin Heidelberg, 2008.

Hans B. Pacejka. *Tyre and vehicle dynamics*. Butterworth-Heinemann, 2002.

F. Pfeiffer and R. Johanni. A concept for manipulator trajectory planning. *IEEE Journal of Robotics and Automation*, 3(2): 115–123, 1987.

S.M. Savaresi and M. Tanelli. *Active braking control systems design for vehicles*. Springer-Verlag, 2010.

Chris Urmson. Realizing self-driving vehicles. In *IEEE Intelligent Vehicles Symposium*, 2012.

Anton T. van Zanten. Evolution of electronic control systems for improving the vehicle dynamic behavior. In *Proceedings of the International Symposium on Advanced Vehicle Control (AVEC)*, pages 7–15, 2002.

D. Verscheure, B. Demeulenaere, J. Swevers, J. De Schutter, and M. Diehl. Time-optimal path tracking for robots: A convex optimization approach. *IEEE Transactions on Automatic Control*, 54(10):2318–2327, 2009.

M. Werling, L. Groll, and G. Bretthauer. Invariant trajectory tracking with a full-size autonomous road vehicle. *IEEE Transactions on Robotics*, 26(4):758–765, 2010.